the concentration required for complete reductive dechlorination (namely 8.5–17 kPa). Chlorinated compounds were added to final aqueous concentrations in the range of 0.47–1.33 mM. Semisolid medium was prepared by adding 0.5% w/w low-melting agarose before autoclaving.

Analytical techniques

The protein content of liquid cultures was estimated as follows. Cells were harvested from 8 ml of culture fluid by centrifugation (10 min, 10,000 *g*). After alkaline cell lysis[22], the Coomassie Plus Protein Assay Reagent Kit (Pierce Biotechnology, Rockford, Illinois) was used in accordance with the manufacturer's recommendations. Spectrophotometric determination at 595 nm was used to quantify protein by comparing the sample absorbance with protein standards of known concentration prepared in the same way as the samples. Chloroethene and ethene concentrations were determined by gas chromatography as described[12].

Electron microscopy

A Zeiss LSM 510 confocal microscope with a Plan-Neofluar objective (100×; numerical aperture, 1.3) was used to obtain micrographs of cell suspensions after staining with acridine orange (15–60 min in 0.01% aqueous solution). Scanning electron microscopy micrographs were obtained with a TOPCON DS-130 field-emission scanning electron microscope with samples staged 'in-lens' and photographed at 20 kV. Samples were prepared as described[23], and coated with chromium (about 1.5 nm thickness) in a Denton DV-602 turbo magnetron sputter system.

Molecular analyses

DNA was extracted from actively growing cultures as described[12]. Real-time PCR to quantify BAV1 cells used a probe targeted to the *Dehalococcoides* 16S rRNA gene, tagged with a 6-carboxyfluorescein reporter fluorochrome on the 5′ end, and *N*,*N*,*N*′,*N*′-tetramethyl-6-carboxyrhodamine quencher on the 3′ end as described previously[12]. Linear calibration curves ($r^2 > 0.99$) were generated, spanning a template concentration range from 6.9×10^2 to 6.9×10^6 16S rRNA gene copies per 30-μl reaction volume by using BAV1 genomic DNA or plasmid DNA containing the 16S rRNA gene from BAV1. Analysis of individual clones with ARDRA was performed as described previously[12,24], except that the PCR-amplified 16S rRNA gene products from each clone were digested for 3 h with enzymes *Hha*I, *Msp*I and *Rsa*I at 37 °C. The reactions were terminated by incubation at 65 °C for 10 min, in accordance with the manufacturer's recommendations (Gibco), and the resulting fragments were resolved by electrophoresis for 2 h on 2.5% low-melting agarose gel (Seaplaque; Cambrex, Rockland, Maine). The fluorescently labelled primer 8F-hex (5′-AGA GTT TGA TCC TGG CTC AG-3′) and unlabelled 1492R (5′-GC(C/T) TAC CTT GTT ACG ACT T-3′) were used to amplify the 16S rRNA gene from pure culture DNA. Fluorescently labelled terminal fragments obtained by digesting the PCR product with *Hha*I, *Msp*I and *Rsa*I were analysed at Michigan State University's Genomics Technology Support Facility. Denaturing gradient gel electrophoresis was performed by Microbial Insights (Rockford, Tennessee) with the use of universal bacterial primers corresponding to *Escherichia coli* positions 341–534 as described[16].

Received 29 January; accepted 29 April 2003; doi:10.1038/nature01717.

1. Kielhorn, J., Melber, C., Wahnschaffe, U., Aitio, A. & Mangelsdof, I. Vinyl chloride: still a cause for concern. *Environ. Health Perspect.* **108,** 579–588 (2000).
2. Mohn, W. W. & Tiedje, J. M. Microbial reductive dehalogenation. *Microbiol. Rev.* **56,** 482–507 (1992).
3. Roberts, A. L. *et al.* Reductive elimination of chlorinated ethylenes by zero-valent metals. *Environ. Sci. Technol.* **30,** 2654–2659 (1996).
4. Vogel, T. M., Criddle, C. S. & McCarty, P. L. Transformation of halogenated aliphatic compounds. *Environ. Sci. Technol.* **21,** 722–736 (1987).
5. US Environmental Protection Agency. Agency for Toxic Substances and Disease Registry, ToxFAQs for chlorinated ethenes; www.atsdr.cdc.gov/tfacts70.html (1996).
6. Coleman, N. V., Mattes, T. E., Gossett, J. M. & Spain, J. C. Phylogenetic and kinetic diversity of aerobic vinyl chloride-assimilating bacteria from contaminated sites. *Appl. Environ. Microbiol.* **68,** 6162–6171 (2002).
7. Coleman, N. V., Mattes, T. E., Gossett, J. M. & Spain, J. C. Biodegradation of *cis*-dichloroethene as the sole carbon source by a β-Proteobacterium. *Appl. Environ. Microbiol.* **68,** 2726–2730 (2002).
8. Holliger, C., Wohlfarth, G. & Diekert, G. Reductive dechlorination in the energy metabolism of anaerobic bacteria. *FEMS Microbiol. Rev.* **22,** 383–398 (1998).
9. Löffler, F. E., Cole, J. R., Ritalahti, K. M. & Tiedje, J. M. in *Dehalogenation: Microbial Processes and Environmental Applications* (eds Häggblom, M. M & Bossert, I. D.) 53–87 (Kluwer Academic, New York, 2003).
10. Maymó-Gatell, X., Chien, Y.-T., Gossett, J. M. & Zinder, S. H. Isolation of a bacterium that reductively dechlorinates tetrachloroethene to ethene. *Science* **276,** 1568–1571 (1997).
11. He, J. *et al.* Acetate versus hydrogen as direct electron donors to stimulate the microbial reductive dechlorination process at chloroethene-contaminated sites. *Environ. Sci. Technol.* **36,** 3945–3952 (2002).
12. He, J., Ritalahti, K. M., Aiello, M. R. & Löffler, F. E. Complete detoxification of vinyl chloride (VC) by an anaerobic enrichment culture and identification of the reductively dechlorinating population as a *Dehalococcoides* population. *Appl. Environ. Microbiol.* **69,** 996–1003 (2003).
13. Adrian, L., Szewzyk, U., Wecke, J. & Görisch, H. Bacterial dehalorespiration with chlorinated benzenes. *Nature* **408,** 580–583 (2000).
14. Hendrickson, E. R. *et al.* Molecular analysis of *Dehalococcoides* 16S ribosomal DNA from chloroethene-contaminated sites throughout North America and Europe. *Appl. Environ. Microbiol.* **68,** 485–495 (2002).
15. Cupples, A. M., Spormann, A. M. & McCarty, P. L. Growth of a *Dehalococcoides*-like microorganism on vinyl chloride and *cis*-dichloroethene as electron acceptors as determined by competitive PCR. *Appl. Environ. Microbiol.* **69,** 953–959 (2003).
16. Duhamel, M. *et al.* Comparison of anaerobic dechlorinating enrichment cultures maintained on tetrachloroethene, trichloroethene, *cis*-dichloroethene and vinyl chloride. *Water Res.* **36,** 4193–4202 (2002).
17. Gribble, G. W. in *Chlorinated Compounds in the Biosphere, Natural Production* (ed. Meyers, R. A.) 972–1035 (Wiley, New York, 1998).
18. Keppler, F., Borchers, R., Pracht, J., Rheinberger, S. & Scholer, H. F. Natural formation of vinyl chloride in the terrestrial environment. *Environ. Sci. Technol.* **36,** 2479–2483 (2002).
19. Lendvay, J. M. *et al.* Bioreactive barriers: bioaugmentation and biostimulation for chlorinated solvent remediation. *Environ. Sci. Technol.* **37,** 1422–1431 (2003).
20. Löffler, F. E., Ritalahti, K. M. & Tiedje, J. M. Dechlorination of chloroethenes is inhibited by 2-bromoethanesulfonate in the absence of methanogens. *Appl. Environ. Microbiol.* **63,** 4982–4985 (1997).
21. Löffler, F. E., Tiedje, J. M. & Sanford, R. A. Fraction of electrons consumed in electron acceptor reduction and hydrogen threshold as indicators of halorespiratory physiology. *Appl. Environ. Microbiol.* **65,** 4049–4056 (1999).
22. Gerhardt, P. (ed.) *Manual of Methods for General Bacteriology* (American Society for Microbiology, Washington DC, 1981).
23. Sung, Y. *et al.* Characterization of two tetrachloroethene-reducing, acetate-oxidizing anaerobic bacteria and their description as *Desulfuromonas michiganensis* sp. nov. *Appl. Environ. Microbiol.* **69,** 2964–2974 (2003).
24. Löffler, F. E., Sun, Q., Li, J. & Tiedje, J. M. 16S rRNA gene-based detection of tetrachloroethene (PCE)-dechlorinating *Desulfuromonas* and *Dehalococcoides* species. *Appl. Environ. Microbiol.* **66,** 1369–1374 (2000).
25. Bunge, M. *et al.* Reductive dehalogenation of chlorinated dioxins by an anaerobic bacterium. *Nature* **421,** 357–360 (2003).

Acknowledgements Electron micrographs were obtained by R. P. Apkarian at the Integrated Microscopy and Microanalytical Facility at Emory University, Atlanta, Georgia. This work was supported by the Strategic Environmental Research and Development Program, and by a National Science Foundation CAREER award to F.E.L.

Competing interests statement The authors declare that they have no competing financial interests.

Correspondence and requests for materials should be addressed to F.E.L. (frank.loeffler@ce.gatech.edu).

Delta-wing function of webbed feet gives hydrodynamic lift for swimming propulsion in birds

L. Christoffer Johansson* & R. Åke Norberg†

** Department of Organismic and Evolutionary Biology, Harvard University, 26 Oxford Street, Cambridge, Massachusetts 02138, USA*
† Department of Zoology, Göteborg University, Box 463, SE-405 30 Göteborg, Sweden

Most foot-propelled swimming birds sweep their webbed feet backwards in a curved path that lies in a plane aligned with the swimming direction. When the foot passes the most outward position, near the beginning of the power stroke, a tangent to the foot trajectory is parallel with the line of swimming and the foot web is perpendicular to it. But later in the stroke the foot takes an increasingly transverse direction, swinging towards the longitudinal axis of the body. Here we show that, early in the power stroke, propulsion is achieved mostly by hydrodynamic drag on the foot, whereas there is a gradual transition into lift-based propulsion later in the stroke. At the shift to lift mode, the attached vortices of the drag-based phase turn into a starting vortex, shed at the trailing edge, and into spiralling leading-edge vortices along the sides of the foot. Because of their delta shape, webbed feet can generate propulsive forces continuously through two successive modes, from drag at the beginning of the stroke, all the way through the transition to predominantly lift later in the stroke.

Foot propulsion in swimming birds has generally been considered to be drag-based, both in surface swimming and during diving[1,2]. Drag is the hydrodynamic force that opposes movement

through a fluid; it is aligned with the movement but acts in the opposite direction. This mode requires that the foot is moved backwards in a still-water frame of reference. The foot must therefore move backwards faster, relative to the bird, than it swims. An entirely different mode of foot-propelled swimming has recently been detected in the great crested grebe (*Podiceps cristatus*)[3,4]. It does not paddle with its feet in a fore-and-aft movement, but instead sweeps its feet outwards–upwards in a transverse plane, perpendicular to the swimming direction. There is no backward movement of the feet relative to the water, so drag cannot be tilted forwards and so is useless for propulsion. Instead, propulsion is based on lift, which here is directed forwards and is nearly perpendicular to the path of the foot[3,4], being by definition normal to the resultant relative flow. There are two functional benefits from using lift rather than pure drag for propulsion. First, with drag-based propulsion, muscle work is done directly against the entire reaction force on the foot, whereas work is done against only a component of it when propulsion is based on lift. And that component is often smaller than the propulsive force. In lift mode it is therefore possible to exploit a propulsive force that is larger than the force against which work is being done. This enhances hydrodynamic efficiency and energy economy. Second, with drag-based propulsion the feet must move backwards in still water, so the bird must sweep its feet faster than it swims. With lift-based propulsion it need not do so, which again improves energy economy and also might allow higher swimming speeds because the sweep velocity of the foot in lift mode need not be nearly as high as the swimming speed.

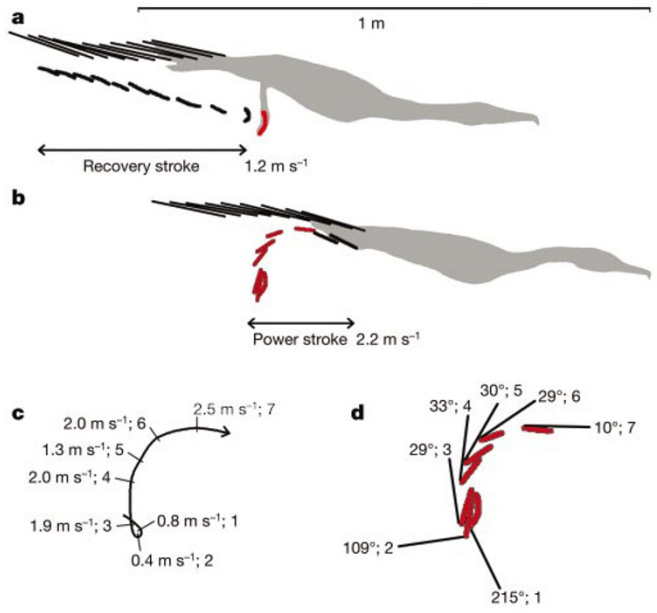

Figure 1 Tracings from a video sequence (separated by 0.02 s) of a foot-stroke cycle of a diving cormorant. Bold lines indicate the position and orientation of the foot, and thin lines show the dorsal side of the tail. **a**, The recovery stroke with the shaded bird at the start of the power stroke. **b**, The power stroke, starting with the same foot position that terminated the upper sequence. The shaded bird is at the end of the power stroke. Acceleration of the body occurs over seven video fields (from 1.2 m s^{-1} at the end of recovery stroke to 2.2 m s^{-1} at position 7 of the power stroke), indicated by the red foot. **c**, **d**, Data for the acceleration phase of **b**. **c**, The instantaneous still-water speed of the trailing edge of the foot is indicated at positions 1–7 along its trajectory. **d**, The instantaneous angle of attack at the trailing edge of the foot is indicated at the same seven foot positions. The drag mode can last, at most, for as long as the foot moves backwards relative to the still water, which it does until slightly after position 3, during which time the angle of attack changes from ~215° to less than 30°. This is 39% of the duration of the power stroke. During the remainder of the power stroke, 61% of the time, the body continues to accelerate forwards, owing entirely to lift.

Here we show that the more conventional fore-and-aft movement of the feet in swimming birds can also generate thrust that is based on hydrodynamic lift. Our results are based on observations and analyses of video films of swimming and diving birds (Fig. 1), and on flow-visualization experiments with a model foot in a simulated power stroke (Fig. 2).

We distinguish three phases of the power stroke. Phase 1 is when the foot performs a largely translatory backward movement near the start of the power stroke. A recirculating wake is formed on the leeward, suction side of the foot, and a closed vortex, surrounding the foot, is rolled up behind its edges. At this stage, the foot moves backwards relative to the water and water meets the foot at nearly right angles to its web. Water is accelerated and drawn backwards along with the foot, over its leeward surface, and the induced flow is bounded by an attached closed vortex. The reaction force on the foot is hydrodynamic drag, directed forwards, opposite to the direction of movement of the foot. It is the useful propulsive force at this stage (Fig. 3).

Because of rotation of the leg, the outer, distal edge of the foot moves faster than its proximal parts, and this velocity gradient creates a stronger suction at the distal edge and a lower pressure within the vortex core there. Water should therefore be drawn towards the foot's trailing edge on the suction side and spiral rearwards in the side-edge vortices, similar to the spanwise, leading-edge flow over flapping insect wings[5]. In this way a rearward flow is set up on the suction side, typical for a wing in lift mode.

Stage 2 of the power stroke occurs after the foot has passed its most outward position: the path curves inwards, towards the longitudinal body axis of the bird. The transverse speed component therefore increases gradually while the backward speed component diminishes. The backward speed component very soon becomes lower than the bird's swimming speed, so the foot no longer moves backwards relative to the water but instead moves forwards with the bird. When this happens, the drag force cannot be tilted forwards, so propulsion is no longer drag-based (Figs 1 and 3).

When the foot starts moving transversely in relation to the swimming direction, it leaves behind the previous, attached, trailing-edge vortex, which now becomes a starting vortex for a drawn-out, U-shaped vortex behind the foot. The vortices that were attached to the sides of the foot in drag mode turn into spiralling leading-edge vortices, which leave stable, trailing tip-vortices behind the outer corners of the foot, as on delta-wings[6,7]. They form the sides of the shed U-shaped vortex (Figs 2 and 3).

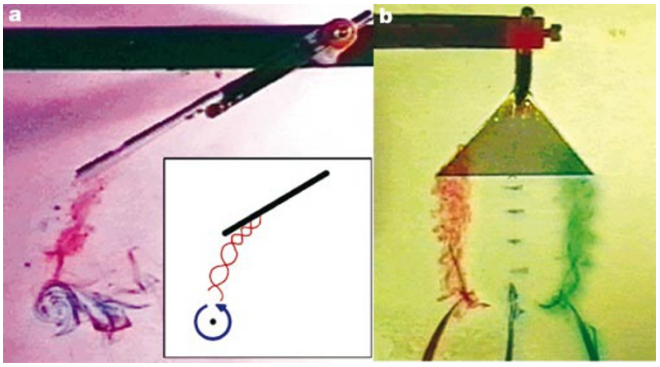

Figure 2 Side and front views of the model foot simulating a power stroke of a swimming bird. **a**, Side view. The foot rotates in a clockwise direction and also translates to the right. **b**, Front view, showing the leeward, suction, side of the foot as seen from the right side in **a**. The flow swirls around the swept-back side edges of the model foot, over to its suction side, where it is entrained in an attached leading-edge vortex that is subsequently shed from the outer corner of the foot to form a spiralling, trailing tip-vortex. The side view also shows a transverse starting vortex left behind in the wake when the model foot moves upwards and to the right.

Circulation is in the same sense as when the vortices were attached to the foot when it translated backwards, in drag mode. Enclosed by the U-shaped vortex is a jet of water flowing backwards at about right angles to the vortex plane. In addition the vortex itself is convected downstream, but at a slower speed than the induced jet (Fig. 3).

Lift production should be facilitated early in the lift phase because there is probably a rearward flow along the suction side of the foot already in drag mode. In addition, the trailing-edge vortex—also developed in drag mode—is just shed as a starting vortex at the transition to lift mode, and the attached side-edge vortices are also built up in drag mode and later turn directly into leading-edge vortices in the lift phase.

When the relative water velocity due to the swimming speed is added vectorially to the velocity due to the foot movement relative to the bird, tangential to the stroke path, the resultant relative water speed is seen to meet the foot from obliquely in front, forming an acute angle of attack with the foot (Fig. 3). This angle depends on the position of the foot in its path and on the relation between the swimming speed and the stroke speed, variables that change throughout the power stroke and along the foot.

The reaction force on the foot is directed obliquely forwards, and is opposite to the direction of the water flow in the jet enclosed by the vortex. It is only because of the production of a lift force that the resultant reaction force gets a forward inclination, owing to which there is a forward force vector. This is the useful propulsive force and it is due entirely to lift. Drag forces on the foot only detract from the propulsive force at this stage (Fig. 3).

In phase 3, at the end of the power stroke the foot is furled and pulled out of the wake and the U-shaped vortex closes after the foot to form an ellipse.

The motion of the model foot in this study is the simple consequence of adding a rotary, sweeping, motion of the foot to the forward velocity of the bird. This suggests that the mechanism described here might also be exploited by other swimming animals with webbed feet or fins. The Δ form occurs in the caudal fins of arrow-worms (phylum Chaetognatha), the caudal and pectoral fins of fishes, in the webbed feet of frogs and most swimming birds, the hind flippers of seals, and the tail flukes of whales and dugongs. In addition, the tail of many birds attains a perfect Δ form when activated and spread, owing to its Λ-notched form when furled. Its delta-wing function has recently been treated theoretically[8] and verified on swallow tails[9]. Hydrofoils and airfoils with a Δ form have thus originated repeatedly and independently by striking evolutionary convergence among widely separate phyletic lines.

A characteristic of a delta-wing is that it is almost unstallable and continues to give large lift forces even at very large angles of attack, although at the penalty of high drag[6,7]. The fluid dynamics of the Δ form is also insensitive to differences in size and speed, as reflected in the Reynolds number[7]. These features enable a Δ-shaped foot or fin to produce large propulsive forces during the entire power stroke when it operates in two successive modes, from pure drag in the beginning of the stroke, all the way through the transition to predominantly lift in later stages. □

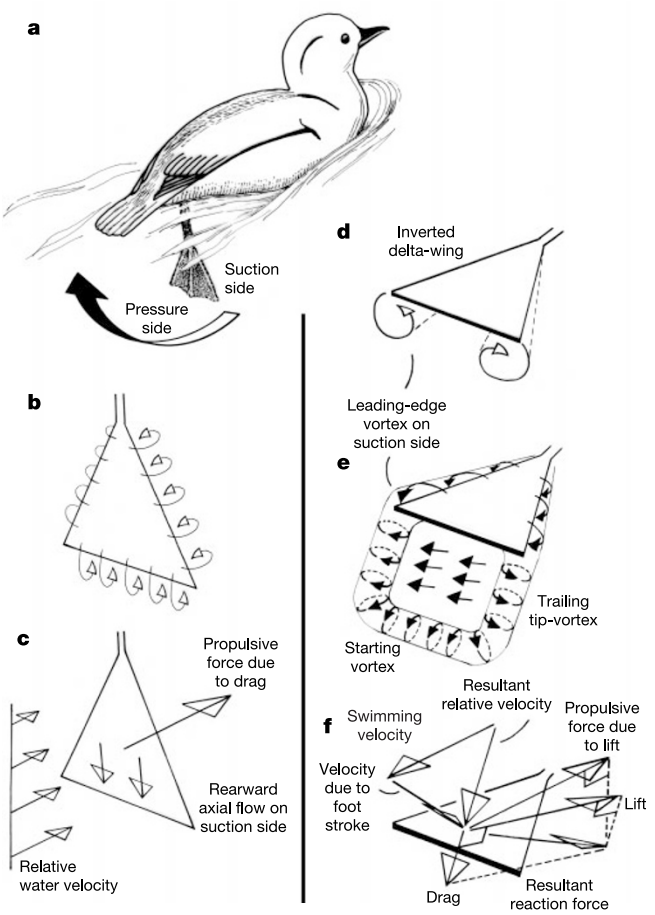

Figure 3 Schematic, generalized representation of flow patterns and forces set up by a webbed foot during a power stroke of a bird in fast swimming. **a**, Definition of suction side and pressure side of the foot in backward motion. The elicited forces are inferred from the induced water flow, as observed in our flow-visualization experiments. **b**, **c**, The foot in drag mode; **d**–**f**, the foot in lift mode at a later stage of the power stroke. The ratio of swimming velocity to foot-stroke velocity used for **f** is roughly as in lift mode at foot position 6 in Fig. 1, and the lift-to-drag ratio is just an example for one phase of the stroke. All velocity and force vectors lie in a common plane aligned with the line of swimming.

Methods

The kinematics of a diving great cormorant (*Phalacrocorax carbo*) was determined by an analysis of video sequences resolved into 50 fields s^{-1}. The velocities of the bird and the feet were estimated by applying a cubic spline fit[10] to the kinematic data. Angles of attack at the distal end of the feet were determined as the angle between the instantaneous, local velocity vector and the foot as seen in lateral view (Fig. 1).

We swept a model foot through water in a movement pattern closely mimicking the natural movement of the diving cormorant. The foot was made of a 2-mm-thick sheet of aluminium, had an isosceles triangular planform with lateral sides 100 mm long, a distal side 85 mm long and a sweepback angle of 65°. This is a simplified, generalized planform for the model foot that is meant to represent the webbed feet of most swimming birds (even though the cormorant foot has a skewed, triangular planform). The paddling movement of the foot was achieved by using a device consisting of two wheels (250 mm diameter) mounted 150 mm apart on a common horizontal axis, which extended 200 mm on the outer side of one of the wheels. The axis was fixed so that it rotated with the wheels. A thin bar was fastened at 90° to the sticking-out free end of the axis, like a single spoke, and the model foot was attached with its leading apex to the distal end of this transverse bar. The entire device was placed on a horizontal ramp inside a water tank. Ramp elevation was adjusted so that the foot became submerged to a suitable depth in water. By adjusting the length of the transverse bar in relation to the radius of the wheels, it was possible to mimic the natural foot movement in a power stroke. The wheels were rolled manually on the ramp as required to simulate a power stroke. The forward movement of the wheel axis corresponded to the bird's swimming speed, and rotation of the axis with the attached model simulated the foot sweep. This combination of a translatory, forward motion of the body and a rotary, backward sweep of the foot characterizes the kinematics of most swimming birds that use a backward power stroke confined to a plane aligned with the line of swimming. We revealed the induced water flow with a dye ejected via plastic tubes with an internal diameter of 1.14 mm; the tubes were attached along the oblique leading edge on the pressure side of the model foot. The flow thus revealed was examined on video films (Fig. 2).

Received 23 December 2002; accepted 22 April 2003; doi:10.1038/nature01695.

1. Blake, R. W. Mechanics of drag-based mechanisms of propulsion in aquatic vertebrates. *Symp. Zool. Soc. Lond.* **48,** 29–52 (1981).
2. Braun, J. & Reif, W.-E. A survey of aquatic locomotion in fishes and tetrapods. *N. Jb. Geol. Paläont. Abh.* **169,** 307–332 (1985).
3. Johansson, L. C. & Lindhe Norberg, U. M. Asymmetric toes aid underwater swimming. *Nature* **407,** 582–583 (2000).
4. Johansson, L. C. & Lindhe Norberg, U. M. Lift-based paddling in diving grebe. *J. Exp. Biol.* **204,** 1687–1696 (2001).
5. Ellington, C. P., van den Berg, C., Willmott, A. P. & Thomas, A. L. R. Leading-edge vortices in insect flight. *Nature* **384,** 626–630 (1996).
6. Katz, J. & Plotkin, A. *Low-speed Aerodynamics* (McGraw-Hill, New York, 1991).

7. Lee, M. & Ho, C.-M. Lift force of delta wings. *Appl. Mech. Rev.* **43,** 209–221 (1990).
8. Thomas, A. L. R. On the aerodynamics of birds' tails. *Phil. Trans. R. Soc. Lond. B* **340,** 361–380 (1993).
9. Norberg, R. Å. Swallow tail streamer is a mechanical device for self-deflection of tail leading edge, enhancing aerodynamic efficiency and flight manoeuvrability. *Proc. R. Soc. Lond. B* **257,** 227–233 (1994).
10. Walker, J. A. QuickSAND. Quick Smoothing and Numerical Differentiation for the Power Macintosh ⟨http://www.usm.maine.edu/~walker/software.html⟩ (1997).

Acknowledgements We thank B. Svensson for building the mechanical experimental device.

Competing interests statement The authors declare that they have no competing financial interests.

Correspondence and requests for materials should be addressed to R.Å.N. (ake.norberg@zool.gu.se).

Chemical and behavioural characterization of the rabbit mammary pheromone

Benoist Schaal*†, Gérard Coureaud*†, Dominique Langlois†‡, Christian Giniès‡, Etienne Sémon‡ & Guy Perrier§

* *Centre Européen des Sciences du Goût, CNRS (fre 2328), 21000 Dijon, France*
‡ *Unité Mixte de Recherche sur les Arômes, Inra, 21000 Dijon, France*
§ *Établissement National d'Enseignement Supérieur Agricole, 21000 Dijon, France*
† *These authors contributed equally to this work*

Mammals owe part of their evolutionary success to the harmonious exchanges of information, energy and immunity between females and their offspring. This functional reciprocity is vital for the survival and normal development of infants, and for the inclusive fitness of parents[1,2]. It is best seen in the intense exchanges taking place around the mother's offering of, and the infant's quest for, milk. All mammalian females have evolved behavioural and sensory methods of stimulating and guiding their inexperienced newborns to their mammae, whereas newborns have coevolved means to respond to them efficiently[3]. Among these cues, maternal odours have repeatedly been shown to be involved[4–6], but the chemical identity and pheromonal nature of these cues have not been definitively characterized until now. Here we focus on the nature of an odour signal emitted by the female rabbit to which newborn pups respond by attraction and oral grasping, and provide a complete chemical and behavioural description of a pheromone of mammary origin in a mammalian species.

The extremely parsimonious strategy of maternal care evolved by the rabbit, *Oryctolagus cuniculus*, offers a unique opportunity to understand the cues that regulate neonatal behaviour in a mammal. The female nurtures her litter for 4–5 min once a day[7] during the 2 weeks after birth: this is therefore less than 0.35% of her time. Because the survival of the pups is conditional on milk intake on the first 2 days of life[8], the pups need a reliable sensory tether for the rapid location of nipples, and competent behaviour to obtain milk successfully in a context of harsh competition between littermates. Rabbit pups are endowed with keen chemosensory and tactile abilities linked with a typical head-searching pattern that ends in the grasping of a nipple within 3–5 s (refs 9, 10). The release of this behaviour is under the main control of chemical cues emitted by lactating females on the nipples[10,11] and in milk[12]. As these skin and milk signals are functionally equivalent[13], we focused our analytical effort on rabbit milk.

The volatiles in milk were extracted, trapped and then desorbed into a gas chromatograph (GC) equipped with a sniffing device, permitting concurrent detection by neonatal rabbits and the flame ionization detector (FID). The pups subjected to such gas chromatography–olfaction (GCO) tests responded either by short-range searching motions of the head directed to the sniff-port, or by attempts to seize it orally (Fig. 1a). The cumulative frequency of both responses allowed us to determine behaviourally active regions on the chromatographic profiles (Fig. 1b). Although some compounds could not be identified because of uninterpretable mass spectra caused by concentration or co-elution problems, most of the GC peaks corresponding to the behavioural peaks were identified by GC–mass spectrometry (GC–MS). The 21 compounds identified were screened for behavioural activity with a bioassay presenting them (aqueous dilution of $1\,\mu g\,ml^{-1}$) on a glass rod (Fig. 2a). One volatile, 2-methylbut-2-enal (2MB2; Fig. 1c), released both responses to a considerably greater extent than any of the other volatiles ($\chi^2 > 50$, $P < 0.001$, for all comparisons) and than the solvent alone ($\chi^2 > 60$, $P < 0.001$) (Fig. 2b).

The pup responsiveness to 2MB2 was dependent on concentration. Its intensity-tuning curve established with the glass-rod test revealed optimal effectiveness between dilution steps $10\,ng\,ml^{-1}$ and $1\,\mu g\,ml^{-1}$ (Fig. 3a). Thus, all subsequent behavioural assays used a constant concentration of 2MB2 ($1\,\mu g\,ml^{-1}$, in water). The 20 remaining compounds isolated from rabbit milk were behaviourally inert at all concentrations between $100\,pg\,ml^{-1}$ and $10\,mg\,ml^{-1}$ (G.C., D.L., G.P. and B.S., unpublished observations).

Additional experiments were conducted to ascertain further that 2MB2 is a key compound in rabbit milk for pups. First, all detectable impurities co-occurring with commercial 2MB2 (namely acetic acid, benzoic acid, 3-methylbut-2-enoic acid and nonanal) were assayed on glass rods and excluded because they had no or negligible effectiveness. Second, when such 2MB2 was assayed by GCO with a polar capillary column, the timing of pup responses corresponded with the retention time of natural 2MB2. Third, the differential separative properties of an apolar GC column were used to check for compounds eluting with 2MB2; in that case too the timing of pup responsiveness matched the retention time of natural 2MB2.

To corroborate the effect of 2MB2, we related its concentration in the milk headspace with the magnitude of the behavioural effect of milk. After standing for 60 min at ambient temperature, rabbit milk loses its effectiveness to evoke pup responsiveness[12,14]. Thus, if 2MB2 is the key compound in milk, the activity loss of the latter would predict a decrease in 2MB2 concentration. The 2MB2 concentration in fresh milk decreased on standing for 30 and 90 min (analysis of variance comparing 0, 30 and 90 min, $F_{2,13} = 8.2$, $P < 0.01$; 0 and 30 min, $F_{1,11} = 7.1$, $P < 0.05$; 30 and 90 min, $F_{1,6} = 4.7$, $P < 0.07$; 0 and 90 min, $F_{1,9} = 36$, $P < 0.01$) and was clearly associated with a drop of neonatal searching–grasping responsiveness ($\chi^2 > 5$, $P < 0.05$ for all comparisons; Fig. 3c). Furthermore, when milk was rendered inactive by headspace extraction (response frequency to milk before and after deodorization, $\chi^2 > 19$, $P < 0.001$ for both responses), its behavioural activity was reinstated by the addition of 2MB2 (response frequency to deodorized versus 2MB2-enriched milks, $\chi^2 > 26$, $P < 0.001$ for both responses; to fresh versus 2MB2-enriched milks, $\chi^2 = 4.8$, $P < 0.05$, for searching; Fig. 3b).

A series of experiments was then undertaken to verify step by step whether 2MB2 carries the psychobiological properties that define a pheromone. Although there is a long-standing semantic debate about the definition of a pheromone in mammals, we used the most restrictive meaning of the concept[15,16]. Thus, five operational criteria were considered to assess whether 2MB2 can qualify as a pheromone: chemical simplicity of the signal; unambiguous, morphologically invariant, and functionally obvious behavioural response of the receiver; high selectivity of stimulus–response coupling; species specificity of reception; and unconditional stimulus–response coupling. A sixth criterion has been added by us that relates to the species specificity of emission of the odour cue.

